TU/e EINDHOVEN UNIVERSITY OF TECHNOLOGY

Toroidal flows in resistive magnetohydrodynamic steady states

Citation for published version (APA):
Kamp, L. P. J., & Montgomery, D. C. (2003). Toroidal flows in resistive magnetohydrodynamic steady states. *Physics of Plasmas*, *10*(1), 157-167. https://doi.org/10.1063/1.1524629

DOI:
10.1063/1.1524629

Document status and date:
Published: 01/01/2003

Document Version:
Publisher's PDF, also known as Version of Record (includes final page, issue and volume numbers)

Please check the document version of this publication:

• A submitted manuscript is the version of the article upon submission and before peer-review. There can be important differences between the submitted version and the official published version of record. People interested in the research are advised to contact the author for the final version of the publication, or visit the DOI to the publisher's website.
• The final author version and the galley proof are versions of the publication after peer review.
• The final published version features the final layout of the paper including the volume, issue and page numbers.

Link to publication

General rights
Copyright and moral rights for the publications made accessible in the public portal are retained by the authors and/or other copyright owners and it is a condition of accessing publications that users recognise and abide by the legal requirements associated with these rights.

• Users may download and print one copy of any publication from the public portal for the purpose of private study or research.
• You may not further distribute the material or use it for any profit-making activity or commercial gain
• You may freely distribute the URL identifying the publication in the public portal.

If the publication is distributed under the terms of Article 25fa of the Dutch Copyright Act, indicated by the "Taverne" license above, please follow below link for the End User Agreement:

www.tue.nl/taverne

Take down policy
If you believe that this document breaches copyright please contact us at:

openaccess@tue.nl

providing details and we will investigate your claim.

Download date: 25. Aug. 2022

Toroidal flows in resistive magnetohydrodynamic steady states

Leon P. Kamp[a)]
Department of Applied Physics, Eindhoven University of Technology, P.O. Box 513, NL-5600 MB Eindhoven, The Netherlands

David C. Montgomery
Department of Physics and Astronomy, Dartmouth College, 6127 Wilder Laboratory, Hanover, New Hampshire 03755-3528

(Received 19 March 2002; accepted 4 October 2002)

Ideal magnetohydrodynamics (MHD) still provides the mathematical framework and the textbook vocabulary in which the possible states of a toroidal plasma are discussed, generally regarded as static equilibria. This is so, despite the increasing realization that virtually all toroidal magnetofluids have nontrivial fluid flows (finite velocity fields) in them. A very different perspective results from nonideal MHD, including both resistivity and viscosity and invoking nonideal boundary conditions. There, it has been shown that if Ohm's law and Faraday's law are given equal importance with force balance, flows are an inevitable consequence of the assumptions of time independence and axisymmetry. Previous treatments of the toroidal steady states for such systems have been based on perturbation theory in which the flow velocity was assumed small, as a consequence of high viscosity (or in dimensionless terms, low Hartmann number H). Here, recently newly available numerical programs are used to lift this limitation and to solve nonlinearly for the allowed steady states of an axisymmetric, current-carrying, toroidal magnetofluid without such an expansion in the Hartmann number. Flow patterns for values of H from $\ll 1$ to $\gg 1$ have been calculated. As H is raised, the flow pattern goes from the predominantly poloidal pair of counter-rotating ''convection cells'' revealed by the perturbation theory to a pattern in which the toroidal kinetic energy of flow considerably exceeds the poloidal kinetic energy. In no case is the flow discovered a simple rotation. © *2003 American Institute of Physics.* [DOI: 10.1063/1.1524629]

I. INTRODUCTION

The possible steady states of a magnetized plasma have been the starting point for nearly all treatments of magnetic fusion confinement and stability.[1–3] Most commonly, it has been the ideal magnetohydrodynamic (MHD) description that has been employed. In the last few years it has become clear that the character of the possible steady states is greatly altered, at least from a theoretical perspective, if nonideal,[4–6] rather than ideal, MHD is employed.[7–10] In the following, nonideal MHD will be taken to mean MHD with viscous and resistive terms included, with Ohm's law and Faraday's law promoted to equal status with the equation of motion, and with some internally consistent set of viscous and resistive boundary conditions—even highly oversimplified ones—enforced.

One of the more striking effects to have emerged concerns the differences between resistive steady states inside a toroid and those inside a straight periodic cylinder with which toroidal geometry is often approximated. In the straight cylinder, it is relatively easy to find steady states including a voltage-driven current distribution which involve no flow (zero velocity-field). However, it has become apparent that in the toroid, virtually all the resistive, driven steady states that can be connected to a realistic resistivity profile involve steady flows with toroidal vorticity. Because of the difficulty of solving the steady-state nonideal MHD equations in toroidal geometry with resistive and viscous boundary conditions, it has been necessary to proceed up to now by perturbation theory, in which the expansion parameter may be variously considered to be the mechanical Reynolds number, the Hartmann number, or the reciprocal of the viscosity.[8–12] Any way the matter is phrased, the solutions have essentially been large-viscosity solutions, in which the flow speed remained small because of size of the viscosity. A characteristic flow pattern emerged, somewhat independently of the shape of the toroidal boundary cross section, and independently of the viscous and resistive boundary conditions imposed: a pair of counter-rotating poloidal vortices or convection cells involving mostly toroidal vorticity.

The purpose of this paper is to report the results of numerical computations that do not require the assumption of small Hartmann number. The method is new, and permits the Hartmann number to range from $\ll 1$ to $\gg 1$. The primary effect to emerge is the appearance of a strong toroidal velocity component that appears in the flow as the Hartmann number is raised and then eventually saturates, when the ratio of its mean square to that of the poloidal flow is considered. By poloidal flow, we mean not a simple poloidal rotation, but rather a flow whose streamlines (often dipolar) lie primarily in a plane perpendicular to the toroidal direction. There are also significant quantitative changes in the nature and geometry of the flow pattern. The focus is on what happens to a given voltage-driven steady state at fixed resistivity and im-

a)Electronic mail: l.p.j.kamp@tue.nl

 © 2003 American Institute of Physics

Downloaded 25 Sep 2008 to 131.155.151.77. Redistribution subject to AIP license or copyright; see http://pop.aip.org/pop/copyright.jsp

posed driving electric field as the viscosity is varied. We do this, because viscosity is one of the most uncertain quantities remaining in high-temperature MHD, both as to the form of the viscous stress tensor and as to the magnitude of the coefficient.[5,6,12] Lack of a sufficiently inclusive theoretical or experimental grasp of magnetized plasma viscosity may be thought of as perhaps the most severe theoretical limitation in fusion MHD at the present time.

We have made several assumptions that we would prefer not to have made, because of our present inability to include them, and we list them now. (1) We have assumed uniform density and incompressibility, to avoid the need for an energy equation and the complications of self-consistent transport coefficients with variable dependencies on density and temperature; we have simply assumed constant values for the coefficients of viscosity and resistivity. (2) We have assumed a simple, Newtonian viscous term and a scalar resistivity, and have avoided confronting the difficulties associated with the Braginskii tensors for viscosity and resistivity. (3) We have assumed stress-free, rather than no-slip, viscous boundary conditions on the velocity field; they may be equally unrealistic approximations for the edge region of a confinement device, but anything more complex involves kinetic theory complications that are presently beyond our reach. (4) We assume axisymmetry throughout. It would be desirable in the future to remove any or all of these four limitations.

Section II contains the MHD equations to be solved. In the Appendix, they are re-expressed, for the case of axisymmetric steady states, in terms of the scalar functions which are computed. Section III is a brief description of the numerical method employed. Section IV summarizes and displays the results of several computations, with an emphasis on the effects of different choices for the assumed magnitude of the viscosity coefficient. Since the cases in Sec. IV have parameters far from close to current laboratory operating regimes, we present in Sec. V two ''realistic'' cases, in which the numbers chosen are taken to correspond as closely as possible to a data set from the first tritium shot in the Joint European Torus (JET). Particularly different are the large values of the Lundquist number S and the small values of the toroidal electric field, which are much larger and smaller than those for the cases reported in Sec. IV. The situation is still ambiguous, however, due to large uncertainties in what should be chosen for the values of the viscosity coefficient. The Braginskii–Balescu[5,6] viscosity tensor formally contains five coefficients of which there are only three basically different ones. The ''ion parallel'' viscosity is an ion thermal speed times an ion collision time, The other two coefficients are down by about one and two powers, respectively, of the ion gyrofrequency times the ion collision time. What we have done is to choose the ''ion parallel'' viscosity coefficient of Braginskii, the largest possible candidate for the viscosity and we have done a calculation with a viscosity coefficient that is a million times smaller. The latter case is intended to illustrate the changes in the flow field when the viscosity coefficient approaches the smallest possible value in the three Braginskii coefficients. Section VI reviews the results and offers some observations on their possible elaboration in experimental settings.

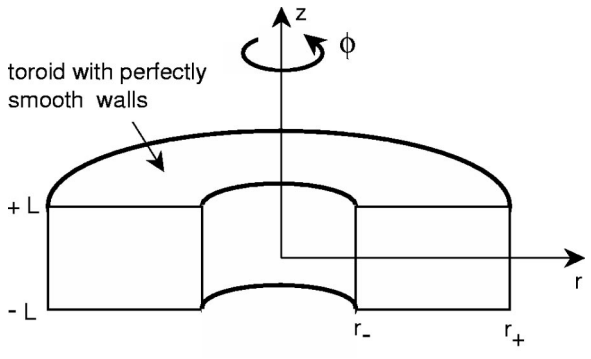

FIG. 1. Geometry of computational model. The toroid has a rectangular cross section with impenetrable, perfectly conducting walls. The magnetofluid occupies the region between the radii r_- and r_+, and $z=-L,+L$. The walls are perfectly smooth.

II. STATEMENT OF THE PROBLEM

We will work in the familiar set of ''Alfvénic'' dimensionless variables for advancing the fluid variables **E** (the electric field), **B** (the magnetic field), **v** (the velocity field), **J** (the electric current density), $\boldsymbol{\omega}$ (the vorticity field), and the scalar pressure p, normalized to the mass density.

With these notations, then, the dimensionless MHD equations of motion for a uniform-density, incompressible, conducting, steady-state fluid are taken to be the following. First, there is mechanical force balance,

$$(\mathbf{v}\cdot\nabla)\mathbf{v}=\mathbf{J}\times\mathbf{B}-\nabla p+\nu\nabla^2\mathbf{v}, \tag{1}$$

where for reasons of tractability we have assumed a simple scalar form for the Newtonian viscous term. The velocity field obeys the incompressibility condition,

$$\nabla\cdot\mathbf{v}=0. \tag{2}$$

Faraday's law reads

$$\nabla\times\mathbf{E}=0. \tag{3}$$

Ohm's law is

$$\mathbf{E}+\mathbf{v}\times\mathbf{B}=\eta\mathbf{J}. \tag{4}$$

Ampère's law says

$$\nabla\times\mathbf{B}=\mathbf{J}. \tag{5}$$

And, finally,

$$\nabla\cdot\mathbf{B}=0. \tag{6}$$

In the dimensionless units used, where velocities are measured in units of the Alfvén speed, ν is the reciprocal of the viscous Lundquist number, M. In terms of laboratory (cgs) units, M is given by $\nu^{-1}=M=C_a\mathcal{L}/\tilde{\nu}$, where C_a is an Alfvén speed based on a typical magnetic field, $\mathcal{L}$ is a characteristic length scale (e.g., the minor radius of the torus), and $\tilde{\nu}$ is the laboratory kinematic viscosity, expressed in cm^2/s. η is the reciprocal of the resistive Lundquist number, S, which in laboratory units is defined by $\eta^{-1}=S=4\pi\tilde{\sigma}C_a\mathcal{L}/c^2$, where $\tilde{\sigma}$ is the cgs electrical conductivity and c is the speed of light. The Hartmann number H is related to M and S through the relation $H=\sqrt{MS}$.

The geometry of the model (see Fig. 1) for which these

Downloaded 25 Sep 2008 to 131.155.151.77. Redistribution subject to AIP license or copyright; see http://pop.aip.org/pop/copyright.jsp

equations may be solved numerically consists of an axisymmetric toroid the axis of symmetry of which coincides with the z-axis in a set of cylindrical polar coordinates (r,φ,z). The midplane of the toroid is the plane $z=0$. The boundaries of the toroidal cross section are taken to be a rectangle. Doing so leads to calculational simplicity, but is not believed to be necessary for the effects we shall describe. The upper and lower boundaries are at $z=L$ and $z=-L$, respectively, and the inner and outer boundaries are at the radii $r=r_-$ and $r=r_+$, respectively. This geometry will be adopted in the present paper. The boundary conditions that have been imposed upon the solutions of the set of Eqs. (1)–(4) are that any tangential viscous stress, and the normal components of **v**, **J**, and **B**, should vanish at the walls. As in the case of the planar-boundary assumption, these boundary conditions are believed not to be uniquely important ones, and are chosen mainly for calculational convenience. One may idealize such a boundary as a perfectly smooth dielectric coating on a perfect conductor.

The source of the driving toroidal electric field is idealized as an axisymmetric, infinitely-long, iron core through which the z-directed magnetic flux is increasing proportionally to the time. This implies a curl-free time-independent toroidal electric field in the φ-direction according to

$$\mathbf{E}_{\text{ext}}(r,z)=E_0\frac{r_0}{r}\hat{\mathbf{i}}_\varphi, \tag{7}$$

where E_0 is a reference value of the electric field at radius $r=r_0$, and $\hat{\mathbf{i}}_\varphi$ is a unit vector in the toroidal (azimuthal) direction. Additionally also a purely toroidal dc magnetic field supported by external poloidal windings around the toroid, is assumed to be present. This magnetic field is curl-free too and is described by

$$\mathbf{B}_{\text{ext}}(r,z)=B_0\frac{r_0}{r}\hat{\mathbf{i}}_\varphi, \tag{8}$$

where B_0 is a reference value of the magnetic field at radius $r=r_0$.

We will ignore the violation of electrodynamics that is implied by the presence of these finite axial electric and magnetic fields inside the perfectly conducting toroidal wall. In real life, the externally maintained electric and magnetic fields would require slits and slots cut into the perfect conductor in order that it might penetrate. That, however, would destroy the the rotational symmetry desired, and make even the problem of finding steady states to perturb prohibitively difficult. So a compromise with the laws of electrodynamics is necessary, even to set up the problem.

III. NUMERICAL SOLUTIONS

Starting from the set of nonideal MHD Eqs. (1)–(6) and using the fact that we consider axisymmetry, we introduce scalar variables according to

$$\mathbf{v}(\mathbf{r},\mathbf{z})=\nabla\psi\times\nabla\varphi+v_\varphi\hat{\mathbf{i}}_\varphi, \tag{9}$$

$$\mathbf{B}(\mathbf{r},\mathbf{z})=\nabla\chi\times\nabla\varphi+\left(B_0\frac{r_0}{r}+B_\varphi\right)\hat{\mathbf{i}}_\varphi, \tag{10}$$

where ψ is the stream function and χ is the flux function. Since there is no time dependence, the gradient of a scalar field may be added to the externally applied electric field,

$$\mathbf{E}(r,z)=E_0\frac{r_0}{r}\hat{\mathbf{i}}_\varphi-\nabla\Phi. \tag{11}$$

With these new variables the electric current density and the vorticity may be expressed as

$$\begin{aligned}\mathbf{J}(r,z)&=\nabla(rB_\varphi)\nabla\varphi-\nabla^2(\chi\nabla\varphi)\\&=\nabla(rB_\varphi)\nabla\varphi-\frac{1}{r}(\Delta^*\chi)\hat{\mathbf{i}}_\varphi,\end{aligned} \tag{12}$$

$$\begin{aligned}\boldsymbol{\omega}(r,z)&=\nabla(rv_\varphi)\nabla\varphi-\nabla^2(\psi\nabla\varphi)\\&=\nabla(rv_\varphi)\nabla\varphi-\frac{1}{r}(\Delta^*\psi)\hat{\mathbf{i}}_\varphi,\end{aligned} \tag{13}$$

where the modified Laplace operator Δ^* is defined by

$$\Delta^*A=\nabla^2A-\frac{2}{r}\frac{\partial A}{\partial r}=\frac{\partial^2A}{\partial r^2}-\frac{1}{r}\frac{\partial A}{\partial r}+\frac{\partial^2A}{\partial z^2}. \tag{14}$$

In the Appendix a coupled set of nonlinear Poisson-like equations is derived for the variables ψ, ω_φ, B_φ, v_φ, χ, and J_φ. This set is then solved numerically using a commercially available software package called FEMLAB.[13] FEMLAB applies the finite element method to our system of partial differential equations in two dimensions in conjunction with adaptive meshing and error control. A numerical solver that is pointed to solving stationary nonlinear equations is used. Because of the symmetry in our problem, we note that all solutions have to be either symmetric (even parity) or antisymmetric (odd parity) with respect to the $z=0$ midplane. B_φ, χ, and J_φ are even functions in z, whereas ψ, ω_φ, and v_φ are odd functions of z. Therefore by considering only, say, the upper half of the toroid we can reduce the amount of numerical calculation by a factor 2. In a typical run the upper half of the toroidal cross section is divided in approximately 10 000 triangles with 5000 nodes to acquire the desired accuracy.

Based on the oddness or evenness of the variable to be solved, we can formulate the following boundary conditions for $z=0$:

$$\begin{aligned}&\left.\frac{\partial B_\varphi}{\partial z}\right|_{z=0}=0,\quad\left.\frac{\partial J_\varphi}{\partial z}\right|_{z=0}=0,\quad\left.\frac{\partial\chi}{\partial z}\right|_{z=0}=0,\\&\psi|_{z=0}=0,\quad\omega_\varphi|_{z=0}=0,\quad v_\varphi|_{z=0}=0.\end{aligned} \tag{15}$$

For the other three boundaries, i.e., $r=r_-$, $r=r_+$ and $z=L$ the conditions upon the solutions are

$$\begin{aligned}&\psi|_{r=r_\pm,z=L}=0,\quad\omega_\varphi|_{r=r_\pm,z=L}=0,\\&B_\varphi|_{r=r_\pm,z=L}=0,\quad\chi|_{r=r_\pm,z=L}=0,\\&J_\varphi|_{r=r_\pm,z=L}=\left.\frac{E_0r_0}{\eta r}\right|_{r=r_\pm},\\&\left.\frac{\partial}{\partial r}\left(\frac{v_\varphi}{r}\right)\right|_{r=r_\pm}=0,\quad\left.\frac{\partial v_\varphi}{\partial z}\right|_{z=L}=0.\end{aligned} \tag{16}$$

Downloaded 25 Sep 2008 to 131.155.151.77. Redistribution subject to AIP license or copyright; see http://pop.aip.org/pop/copyright.jsp

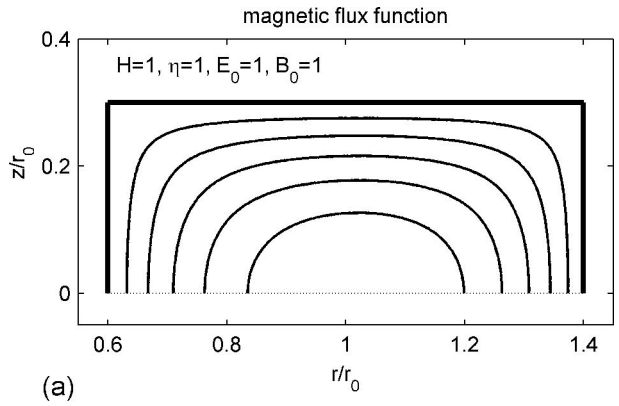

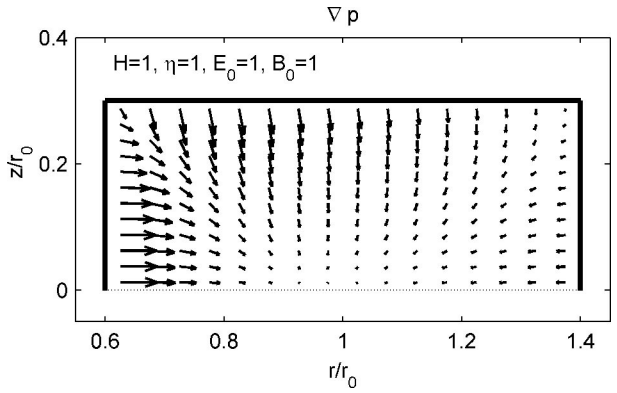

FIG. 3. Vector plot of ∇p for the same set of parameters as in Fig. 2.

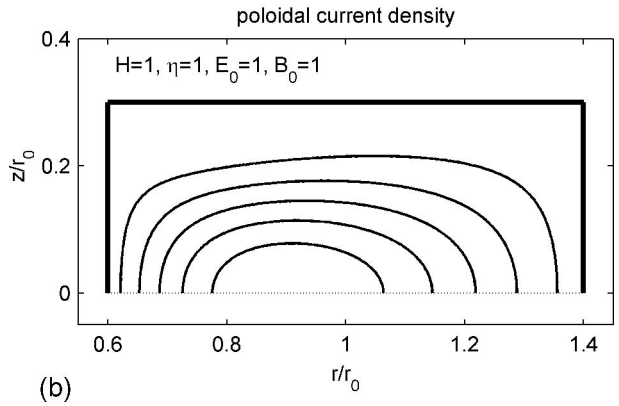

FIG. 2. (a) A plot of the poloidal magnetic field lines for $r_-/r_0=0.6$, $r_+/r_0=1.4$, $L/r_0=0.3$, and $H=1$. (b) Streamlines of the poloidal current density for the same set of parameters as in (a).

As explained in the Appendix, solutions for **v**, **B**, and **J** can be calculated without *a priori* knowledge of the pressure p and the electric potential Φ. The latter follow from (1) and (4), respectively, and are determined up to an additive constant [see Eqs. (A9) and (A10)].

IV. RESULTS

From the set of equations to be solved, i.e., (A14)–(A19) of the Appendix, it should be clear that apart from choosing numerical values for the boundaries of the rectangular cross section of the toroid, there are four parameters to vary. These are the values of the externally maintained fields E_0 and B_0 and the values of the electrical conductivity η and the Hartmann number H, which is a measure for the viscosity of the magnetofluid. In the present paper the emphasis will be on the influence of lowering the viscosity on the flow fields in poloidal and toroidal directions keeping the electrical conductivity and and the externally imposed fields constant. In effect this means that the Hartmann number is increased. In what follows we will take $E_0=1=B_0$ and $\eta=1$ unless otherwise specified.

In Fig. 2 we show a typical example of a run of FEMLAB with the Hartmann number taken to be unity. We should note that because of the symmetries about the midplane $z=0$, we are showing only the upper half of the toroidal cross section in these and similar figures; the variables in the lower half can be inferred from obvious symmetries. Contour plots of the magnetic flux function χ and the poloidal current density stream function rB_φ using $x_-=r_-/r_0=0.6$, $x_+=r_+/r_0=1.4$, and $y_0=L/r_0=0.3$ appear in this figure. Note the slight outward shift of the magnetic surfaces with respect to the center of the toroidal cross section. This is not too different from the ''Shafranov shift'' found in ideal MHD equilibria. The pinch ratio, being the surface-averaged poloidal magnetic field divided by the mean toroidal magnetic field for this set of parameters, is found to be 0.171. We also calculated the ratio of the total kinetic energy to the total magnetic energy, the latter calculated with and without the externally imposed toroidal magnetic field (8) included. For the current set of parameters these numbers are found to be, respectively, 1.29×10^{-8} and 8.39×10^{-7}.

Figure 3 contains a vector plot of ∇p calculated from Eq. (A9) for the same set of parameters as in Fig. 2. At the rectangular toroidal boundary, ∇p has a finite tangential component, indicating that the bounding wall is not an isobaric surface. However, note that tangential stress at the boundary is absent since we require the toroidal vorticity to vanish there.

As mentioned before, up to now the set of equations given in the Appendix could only be solved by perturbation theory[8,9] based on the assumed smallness of the Hartmann number. Using FEMLAB we recalculated these so-called ''slow-flow'' solutions **v**, **B**, and **J** for a small value of the Hartmann number. Contour and surface plots thus obtained of the toroidal vorticity ω_φ, the velocity stream function ψ, and the toroidal velocity v_φ are given in Fig. 4 for the same parameters used in Figs. 2 and 3, but with $H=0.1$.

The next set of figures is devoted to the behavior of the poloidal and toroidal velocity fields for increasing values of the Hartmann number. Again for $x_-=r_-/r_0=0.6$, $x_+=r_+/r_0=1.4$, and $y_0=L/r_0=0.3$ we show combinations of contour and surface plots of the toroidal vorticity ω_φ, the velocity stream function ψ, and the toroidal velocity v_φ for $H=1$ (Fig. 5), $H=40$ (Fig. 6), $H=100$ (Fig. 7), and for $H=500$ (Fig. 8).

In all the color plots the color is a measure for the value of the relevant toroidal quantity, blue meaning a low (possibly negative) value and red meaning a high value. Since the

Downloaded 25 Sep 2008 to 131.155.151.77. Redistribution subject to AIP license or copyright; see http://pop.aip.org/pop/copyright.jsp

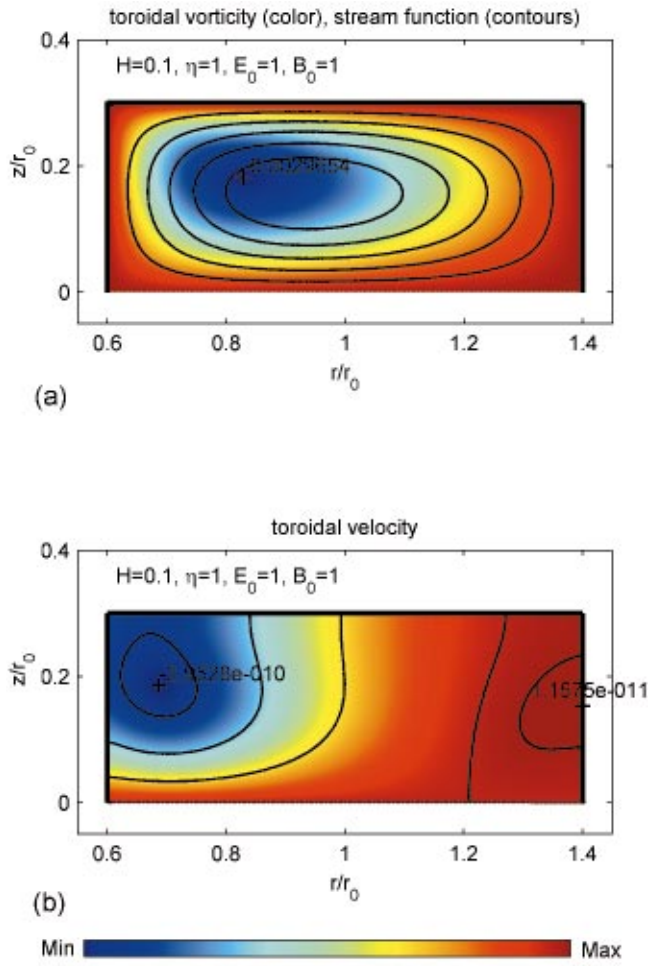

FIG. 4. (Color) (a) Color plot of the toroidal vorticity ω_φ combined with contours of the stream function ψ. A marker indicates the extreme value of the toroidal vorticity. (b) Color plot of the toroidal velocity v_φ. Markers indicate the maximum and minimum values of the toroidal velocity. Both plots for $r_-/r_0=0.6$, $r_+/r_0=1.4$, $L/r_0=0.3$, and $H=0.1$. The pinch ratio for this case is 0.116 and the ratio of total kinetic and magnetic energy with and without the externally applied toroidal magnetic field included, is, respectively, 1.29×10^{-12} and 8.40×10^{-11}. The color bar indicates the color coding between the extreme values as they are marked in the plots.

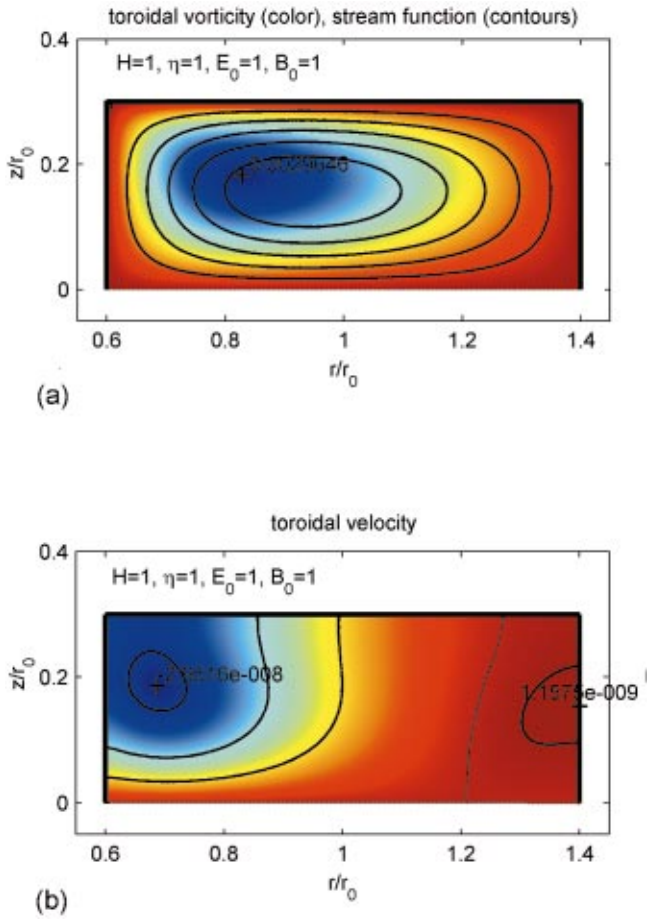

FIG. 5. (Color) Same as Fig. 4 but with $H=1$. The pinch ratio for this case is 0.171 and the ratio of total kinetic and magnetic energy with and without the externally applied toroidal magnetic field included, is, respectively, 1.29×10^{-8} and 8.39×10^{-7}.

value corresponding to a certain color is not the same in all the color plots, we have placed minimum and maximum markers in them. In the toroidal vorticity plots we have indicated by a marker where this quantity attains its minimum value. Toroidal vorticity in the upper half of the toroidal cross section is for the range of Hartmann numbers we investigated always negative inside the bounding wall meaning that it becomes maximum at the wall of the toroid. Extreme values of toroidal velocity are also indicated by markers.

When increasing the Hartmann number we note that the topology of the poloidal flow field does not change very much. As in the previously investigated ''slow-flow'' cases,[8,9] the poloidal flow still is characterized by paired convection-like cells resembling a ''double smoke ring'' configuration. For the toroidal flow the situation is quite different. For a low Hartmann number (see Fig. 4) v_φ changes sign when crossing the toroidal cross section horizontally. Adding this toroidal velocity component vectorially to the (larger) poloidal flow results in a steady-state streamline configuration that topologically is equivalent to helices, which circle the toroid in alternate senses, amounting to what are essentially four ''convection cells.'' For low Hartmann numbers the toroidal speed scales with the reciprocal of the dimensionless viscosity ν. Figures 5–8 show that for increasing Hartmann number, the toroidal flow speed eventually takes over in overall magnitude resulting in a situation in which the total flow is predominantly in the toroidal direction. For even larger values of H, the toroidal flow develops into a double jet structure (see Fig. 8) giving rise again to essentially four ''convection cells'' each of which amounts to helical stream lines. Finally, we emphasize that these helical stream lines are not parallel to the magnetic field **B**.

Our computations indicate that increasing the Hartmann number, keeping the electrical conductivity constant (which amounts to lowering the viscosity) as well as keeping E_0 and B_0 constant, has almost no effect on the total magnetic energy in the toroid. However, kinetic energy rapidly increases in that case, leading to the rise in energy ratios as indicated in the captions of Figs. 4–8. In fact from the ''slow-flow'' Eq. (A23)–(A25) together with Eq. (A11) it may be estimated that the ratio of kinetic energy and magnetic energy in the toroid scales with H^4 as $H\to0$.

Downloaded 25 Sep 2008 to 131.155.151.77. Redistribution subject to AIP license or copyright; see http://pop.aip.org/pop/copyright.jsp

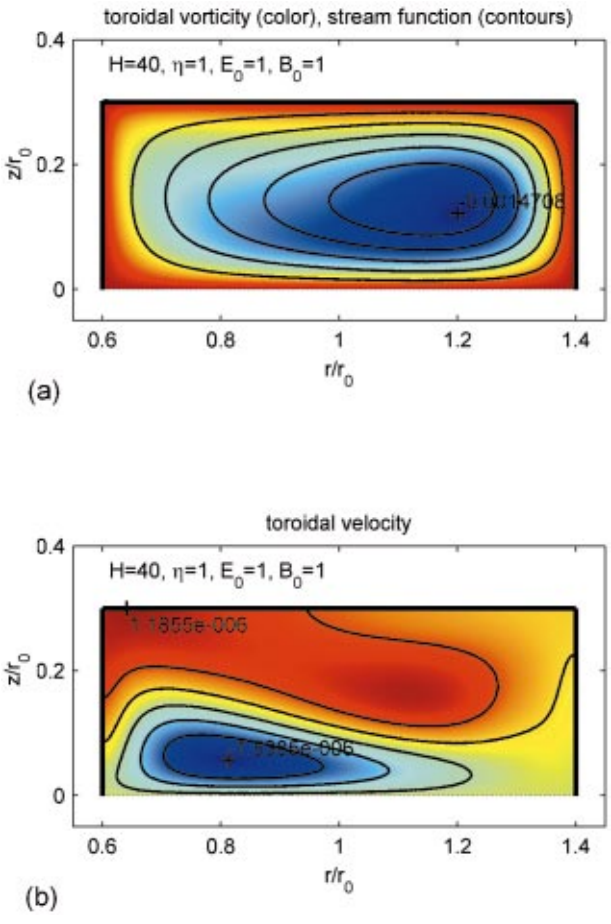

FIG. 6. (Color) Same as Fig. 4 but with $H=40$. The pinch ratio for this case is 0.171 and the ratio of total kinetic and magnetic energy with and without the externally applied toroidal magnetic field included, is, respectively, 0.014 and 0.893.

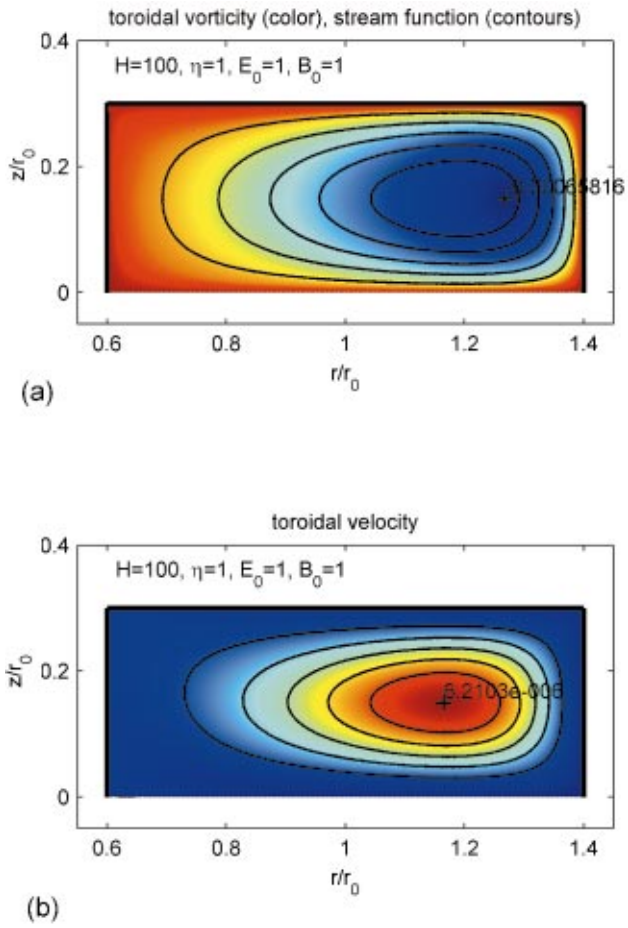

FIG. 7. (Color) Same as Fig. 4 but with $H=100$. The pinch ratio for this case is 0.170 and the ratio of total kinetic and magnetic energy with and without the externally applied toroidal magnetic field included, is, respectively, 0.109 and 7.20.

Figure 9 shows the ratio of kinetic energies contained in the toroidal and poloidal components of the flow vs an increasing Hartmann number for $E_0=1=B_0$ and for $E_0=10=B_0$. In order to have both plots in the same figure, what is actually plotted is this ratio divided by B_0^2. For $E_0=10=B_0$ we see that for sufficiently low viscosity toroidal flow overtakes the poloidal one.

The main conclusion from Figs. 4–8 is that the flow pattern goes from the previously identified pair of counter rotating toroidal vortices[8] (dipolar poloidal convection cells) to a pattern in which the toroidal component of the flow becomes important too.

V. A "REALISTIC" PARAMETER SET

The numbers chosen to present the results of Sec. IV are not close to the operating regimes of current toroidal confinement devices. In particular, the values of the Lundquist number S are not large enough, and the toroidal electric field is much too large. Here, we present results from a run in which the plasma parameters are chosen to be close to those of the first tritium shot in the JET.[14] The value of the toroidal voltage is chosen to be 1 V, and S is then chosen to give a plausible toroidal current of 3.1 MA. For the imposed toroidal magnetic field, we take 28 kG. The cross section of the toroid is still approximated as rectangular, ranging in radius between radii of 2.4 m and 3.6 m, and between values of z of -0.9 m and $+0.9$ m. The plasma is assumed to be deuterium, with an electron density of 3.6×10^{19} per cubic meter and an electron temperature of 10 keV. The ion temperature is assumed to be 18 keV. Following the tabulated formulas in the NRL handbook[15] for collision times and transport coefficients, this gives too large a value of S (1.4×10^{10}), and we are led instead to a Lundquist number S of 1.8×10^{8}, in order to achieve the 3.1 MA toroidal current, neglecting the $\mathbf{v}\times\mathbf{B}$ contribution in Ohm's law. The validity of the latter has been verified numerically. This lower value of S may be attributed to an anomalous resistivity, outside the MHD framework.

The viscosity is of course uncertain within orders of magnitude, experimentally and theoretically. We first make the somewhat arbitrary choice of the "ion parallel" viscosity, the biggest of the three Braginskii–Balescu coefficients. This leads to a laboratory kinematic viscosity $\tilde{\nu}$ of 1.25×10^{15} cm^2/s. The resulting viscous Lundquist number is then $M=8.64\times10^{-5}$, with a Hartmann number of about 125. The dimensionless parameters E_0 and B_0 of previous subsections are now 2.5×10^{-9} and 1.0, respectively, and the dimensionless length r_0 is 2.0. The resulting pinch ratio is 0.152. Figures 10(a) and 10(b) are color plots of toroidal

Downloaded 25 Sep 2008 to 131.155.151.77. Redistribution subject to AIP license or copyright; see http://pop.aip.org/pop/copyright.jsp

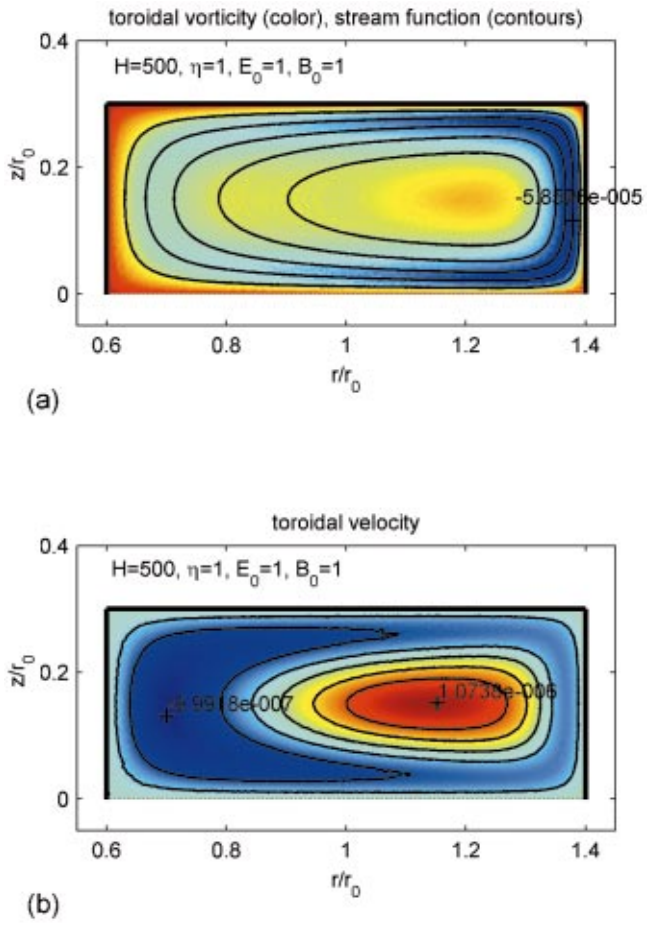

FIG. 8. (Color) Same as Fig. 4 but with $H=500$. The pinch ratio for this case is 0.169 and the ratio of total kinetic and magnetic energy with and without the externally applied toroidal magnetic field included, is, respectively, 0.281 and 18.72.

vorticity [color in Fig. 10(a)] and stream function [contours in Fig. 10(a)], and toroidal velocity [color in Fig. 10(b)]. Root mean square values for flow speeds in the toroidal direction are about 0.84 cm/s and in the poloidal direction,

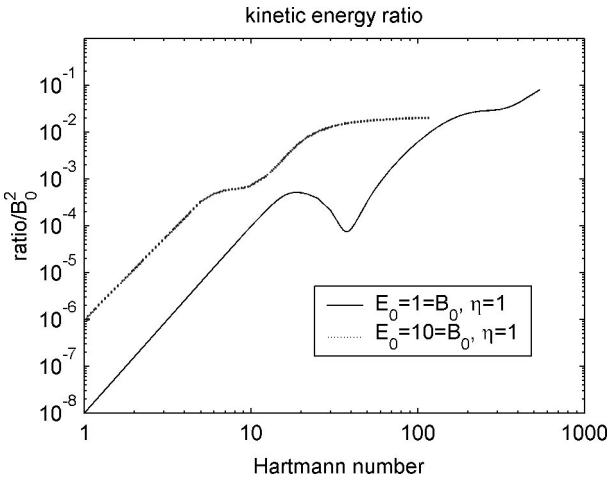

FIG. 9. Plotted here is the ratio of kinetic energy contained in the toroidal component of the flow to that contained in the poloidal part of it for two different values of E_0 and B_0, $r_-/r_0=0.6$, $r_+/r_0=1.4$, $L/r_0=0.3$ and for increasing Hartmann number. In order to have both plots in the same figure, what is actually plotted is this ratio divided by B_0^2. Note that for $E_0=10=B_0$ the toroidal flow component becomes dominant for $H\geqslant 25$.

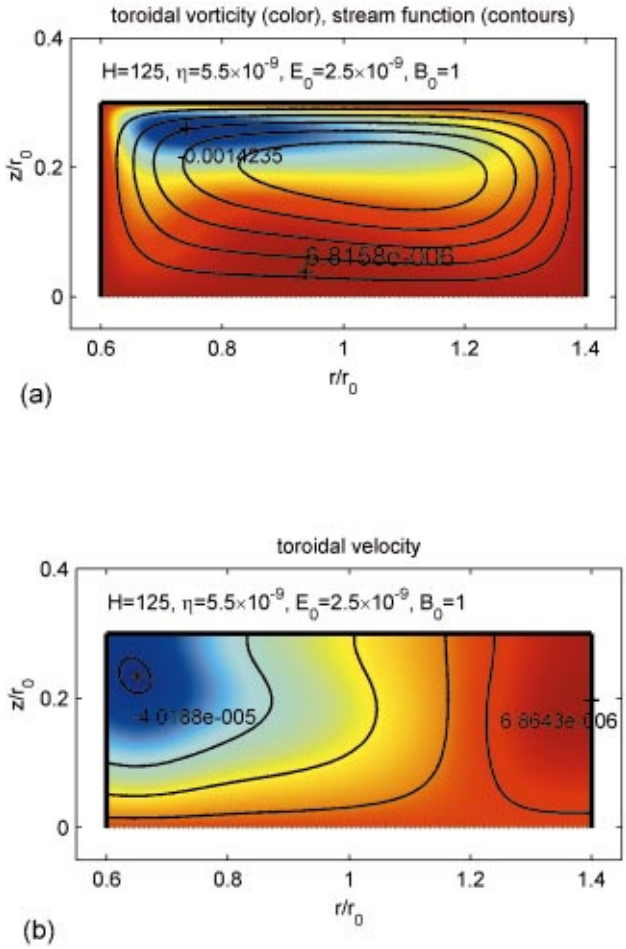

FIG. 10. (Color) Same as Fig 4 but with "realistic" parameters, i.e., $S=1.80\times10^8$, $M=8.64\times10^{-5}$, resulting in a Hartmann number of 125. The total toroidal current and the mean of the total toroidal magnetic field that result from these parameters are 3.04 MA and 29.86 kG, respectively. The pinch ratio is 0.152.

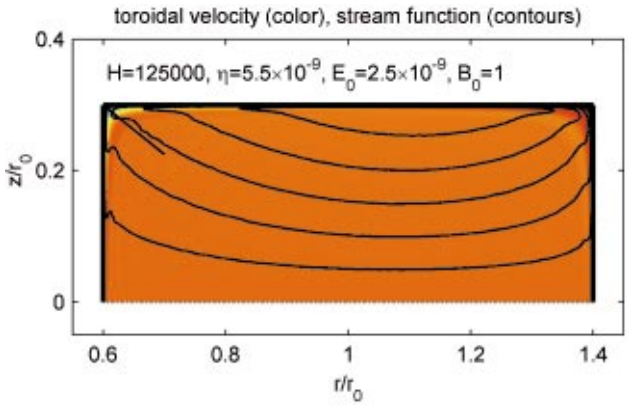

FIG. 11. (Color) Contour plot of the stream function combined with a color plot of the toroidal velocity. This plot is for $r_-/r_0=0.6$, $r_+/r_0=1.4$, $L/r_0=0.3$, and "realistic" parameters $S=1.80\times10^8$ and $H=125\,000$. The straight-line element between $r/r_0=0.7$, $z/r_0=0.225$, and $r/r_0=0.6$, $z/r_0=0.3$ crosses the boundary layer near the wall of the torus. Plots of the boundary layer behavior in the stream function and in the toroidal velocity when traversing the cross section of the torus along this line towards the wall of the torus appear in Fig. 12.

Downloaded 25 Sep 2008 to 131.155.151.77. Redistribution subject to AIP license or copyright; see http://pop.aip.org/pop/copyright.jsp

0.96 cm/s. Maximum flow speeds in the toroidal and poloidal direction are 2.5 cm/s and 2.9 cm/s, respectively. The toroidal energy of flow is about 0.77 times the poloidal kinetic energy of flow.

It is to be stressed that these modest flow speeds are a direct consequence of our having picked the largest possibility in sight for a viscosity coefficient. Alternatively, one could also have chosen the smallest of the three Braginskii–Balescu viscosity coefficients. This so-called transverse viscosity is about $(\omega_{ci}\tau_i)^2$ times smaller than the "ion parallel" viscosity. Here ω_{ci} is the ion cyclotron frequency and τ_i is the ion collision time. For the JET, $\omega_{ci}\tau_i \approx 10^6$. The Hartmann number that follows from this smallest value of a viscosity coefficient is about a million times larger than the one that follows from the "ion parallel" viscosity, i.e., $H=125\times10^6$. At this moment we are unable to perform a numerical calculation for such a large value of the Hartmann number. The main reason for that will become clear in the rest of this section where we present results of a calculation for a value of H for which FEMLAB still gives reliable results, namely, $H=125\,000$. The other parameters are kept to the same values as they had in the $H=125$ calculation above.

Figure 11 is a combination of a contour plot of the stream function and a color plot of the toroidal velocity for the high-H computation. A striking feature of the flow now is that although in the interior of the torus flow speeds do not differ much from the ones of the previous $H=125$ computation (poloidal speeds are typically 0.7 cm/s and toroidal speeds are typically 1.5 cm/s in the interior) large flow speeds occur very close to the wall. Our calculations show that this feature becomes more prominent when the Hartmann number increases. Lowering the viscosity leads near the wall to a narrowing layer of increasing flow speed, i.e., a boundary layer. In the boundary layer large gradients in the stream function and in the toroidal velocity develop. This boundary layer behavior is illustrated in Fig. 12 that shows typical cross-section plots of the stream function and of the toroidal velocity when approaching the wall of the torus by traversing the plasma from $r/r_0=0.7$, $z/r_0=0.225$ to $r/r_0=0.6$, $z/r_0=0.3$. The maximum flow speeds that are attained at the wall in the poloidal and toroidal direction are 122 cm/s and 225 cm/s, respectively.

The narrowing of the boundary layer combined with an increase in gradients for increasing Hartmann number is the main reason for not being able to perform a numerical calculation for the smallest possible value of the three Braginskii–Balescu viscosity coefficients. Resolving the ever increasing fine structure of the flow field near the wall of the torus when the viscosity is lowered by again three orders of magnitude is currently beyond our numerical capabilities.

Finally, it is to be noted that the structure of the boundary layer is likely to be sensitive to the type of boundary conditions that are imposed upon the solutions (e.g., stress-free vs no-slip boundary conditions) and also to the shape of the boundary (rectangular versus circular). A comparison of this small viscosity computation with MHD calculations in which the viscosity is set to zero from the outset is tricky. Setting $\nu=0$ in Eq. (1) lowers the order of our system of differential equations, and it ought to be impossible then to impose as many boundary conditions as we did in the present paper.

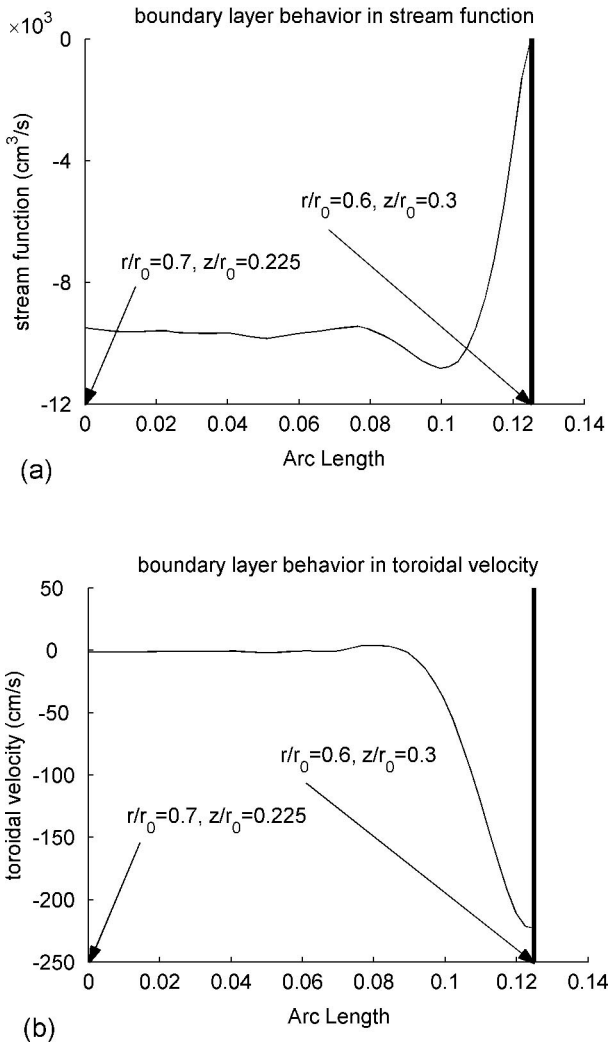

FIG. 12. Typical cross-section plots of the boundary layer near the wall of the torus for the same set of parameters as in Fig. 11. (a) Plotted is the value of stream function in cm^3/s when approaching the wall of the torus along the straight-line element depicted in Fig. 11 starting at $r/r_0=0.7$, $z/r_0=0.225$ and ending at $r/r_0=0.6$, $z/r_0=0.3$. (b) Same as (a) but now the value of the toroidal speed in cm/s is plotted.

VI. CONCLUSIONS

By using newly available numerical methods (FEMLAB), we have lifted the restriction to low Hartmann number (high viscosity) that had limited our earlier attempts at calculating the velocity fields associated with voltage-driven, nonideal, toroidal, steady states in a rigidly wall-bounded magnetofluid. The emergent flow pattern ("weather map") has been characterized for a range of Hartmann numbers, ranging from $\ll 1$ to $\gg 1$. The flows have arisen from giving Faraday's law and Ohm's law equal status with force balance in the dynamics. There are both toroidal and poloidal components of the flows for finite Hartmann numbers, and neither may be characterized as a simple rotation. As the Hartmann number is raised, the toroidal component becomes important,

Downloaded 25 Sep 2008 to 131.155.151.77. Redistribution subject to AIP license or copyright; see http://pop.aip.org/pop/copyright.jsp

and eventually, for sufficiently large externally imposed fields, overtakes the poloidal one in magnitude. If $H \ll 1$, which has been dealt with in perturbation theory,[8–12] the poloidal flow is due to a torque that comes from the fact that the $\mathbf{J}\times\mathbf{B}$ force (where $\mathbf{B}$ is the poloidal part of the magnetic field and $\mathbf{J}$ is the toroidal component of the current density) is no longer directed toward the geometical center of the cross section, the way it is in cylindrical geometry. This means that there is a local nonvanishing $\mathbf{r}\times(\mathbf{J}\times\mathbf{B})$ torque density that tries to twist the plasma in a poloidal plane. It succeeds and does work steadily against viscosity, creating a steady-state velocity dipolar pattern in the direction expected. The situation becomes less easy to see through as the viscosity is lowered, thereby raising H, increasing the velocity magnitude, and producing significant poloidal currents. Apparently what happens is that a component of local torque density develops which tries to twist the plasma in a toroidal direction as well, becoming more and more effective as the viscosity is lowered (i.e., as H goes up). We must admit an incomplete ability to visualize the torque and force balances that arise in this case, though we do believe the numerical results.

Though the examples given in Sec. IV are academic, and intended only to illustrate the fundamental phenomenon and its variation with Hartmann number, the two examples of Sec. V come from choosing numbers as close as possible to a realistic large tokamak parameter set. It is to be stressed that the relatively modest typical flow speeds (1 cm/s) found in the first example for the largest possible estimate for viscosity amount to a sort of lower bound on the internal velocities. The highest-computable-H results ($H=125\,000$) in the second example of Sec. V show flow speeds in excess of 100 cm/s in a boundary layer near the toroidal wall; as far as we know, this boundary layer behavior is new and has not appeared in this context before. Finally, it is perhaps unnecessary to mention that the analytic estimates we have for such quantities as conductivity and viscosity originate in Chapman–Enskog calculations for collision dominated plasmas, which likely do not represent well high-temperature behavior in the JET.

Nevertheless, we believe that to the extent that MHD is relevant to high-temperature confinement at all, the predictions of the presence of both the steady-state toroidal and poloidal flows are solid. The analytical or computational estimates cannot be sharpened up without more reliable numbers for viscosity.

Stress-free mechanical boundary conditions at the toroidal boundary have been employed. It is not clear what differences would arise from some other choice of velocity-field boundary conditions, such as no-slip ones, but it seems certain that there would be some. Any tractable idealization of the velocity field at the wall seems unlikely to do full justice to the complicated mechanical interaction that must occur at a limiter or divertor operated tokamak wall, but it still seems of use to have at least a few solved problems in the catalog of MHD steady states. Up to now, these have largely been ideal steady states, which are seen to be qualitatively different in character.

It has been clear for some time that flows seem likely to be an inherent and important part of any toroidal MHD steady state, and present inability to diagnose in detail the character of those flows stands as a serious experimental impediment in confinement research. We see the most severe theoretical limitation as the absence of manageable approximations to the viscous stress tensor that go beyond the simple, scalar Newtonian viscosity terms used here. Much if not most of the extant stability and turbulent-transition literature will likely need to be modified when and if reliable viscous terms can be identified and agreed upon. But as in the case of neutral fluids, it seems eminently reasonable that a dissipative magnetofluid experiencing rather complex external forces will also experience mechanical motions.

ACKNOWLEDGMENTS

The work described here was financially supported by the Netherlands Organization for Scientific Research (NWO) and in part by the U.S. Department of Energy. L.P.K. acknowledges the hospitality of the Department of Physics and Astronomy of Dartmouth College. The work of one of us (D.C.M.) was supported in part at the Eindhoven University of Technology, under the auspices of the J.M. Burgers Centrum.

APPENDIX: EQUATIONS TO BE SOLVED

In this appendix we will rewrite the set of nonideal MHD equations (1)–(6). We start by taking the toroidal part of Eq. (13). This results in

$$\Delta^*\psi = -r\omega_\varphi . \tag{A1}$$

Next consider the vorticity equation that is obtained from taking the curl of the force balance Eq. (1),

$$\nu\nabla^2\boldsymbol{\omega} = \nabla\times(\boldsymbol{\omega}\times\mathbf{v}+\mathbf{J}\times\mathbf{B}). \tag{A2}$$

Taking the toroidal part of this equation yields

$$\begin{aligned}\nu\Delta^*(r\omega_\varphi)\nabla\varphi = {}& \nabla(rv_\varphi)\times\nabla\left(\frac{v_\varphi}{r}\right)+\nabla\left(\frac{\omega_\varphi}{r}\right)\times\nabla(\psi)\\ & +\nabla\left(\frac{B_\varphi}{r}+\frac{B_0 r_0}{r^2}\right)\times\nabla(rB_\varphi)\\ & +\nabla\chi\times\nabla\left(\frac{J_\varphi}{r}\right).\end{aligned} \tag{A3}$$

The curl of the poloidal part of Ohm's law (4) leads to the following equation for B_φ:

$$\eta\Delta^*(rB_\varphi)\nabla\varphi = \nabla\left(\frac{B_\varphi}{r}+\frac{B_0 r_0}{r^2}\right)\times\nabla\psi-\nabla\left(\frac{v_\varphi}{r}\right)\times\nabla\chi. \tag{A4}$$

An equation for v_φ is obtained by rewriting the force balance equation (1) as follows:

$$\nu\nabla^2\mathbf{v} = \nabla(p+\tfrac{1}{2}v^2)+\boldsymbol{\omega}\times\mathbf{v}-\mathbf{J}\times\mathbf{B}. \tag{A5}$$

The toroidal part of this equation gives

$$\nu\Delta^*(rv_\varphi) = [\nabla\chi\times\nabla(rB_\varphi)-\nabla\psi\times\nabla(rv_\varphi)]\cdot\nabla\varphi. \tag{A6}$$

The toroidal part of Eq. (12) reults in

Downloaded 25 Sep 2008 to 131.155.151.77. Redistribution subject to AIP license or copyright; see http://pop.aip.org/pop/copyright.jsp

$$\Delta^*\chi = -rJ_\varphi, \tag{A7}$$

where the toroidal current density follows from the toroidal part of Ohm's law,

$$\eta r J_\varphi = E_0 \frac{r_0}{r} - \frac{\nabla\chi\times\nabla\psi}{r}\cdot\nabla\varphi. \tag{A8}$$

Equations (A1), (A3), (A4), (A6), and (A7) form a set of coupled, nonlinear Poisson-like equations for the scalar variables ψ, $r\omega_\varphi$, rB_φ, rv_φ, and χ to be supplemented with expression (A8) for J_φ. Note that these equations can be solved without *a priori* knowing the pressure p and the scalar potential Φ. Once this is done ∇p follows from the force balance equation (1) rewritten as follows:

$$\nabla p = \nu\nabla^2\mathbf{v} - \nabla\left(\frac{v^2}{2}\right) - \boldsymbol{\omega}\times\mathbf{v} + \mathbf{J}\times\mathbf{B}. \tag{A9}$$

This determines the pressure up to an additive constant. In a similar fashion Φ follows out of the poloidal part of Ohm's law, i.e.,

$$\nabla\Phi = \mathbf{v}\times\mathbf{B} - \eta\nabla(rB_\varphi)\times\nabla\varphi, \tag{A10}$$

in which we have used Ampère's law (5) to replace the poloidal current density in terms of the toroidal magnetic field.

The final step is to introduce new variables according to

$$\begin{aligned} &u_1 = \frac{\psi}{r_0}, \quad u_2 = r_0 r\omega_\varphi, \quad u_3 = \frac{rB_\varphi}{I_b} + 1, \\ &u_4 = \frac{rv_\varphi}{I_b}, \quad u_5 = \frac{\chi}{r_0}, \quad u_6 = r_0 rJ_\varphi - I_e, \end{aligned} \tag{A11}$$

where

$$I_e = \frac{r_0^2 E_0}{\eta} \text{ and } I_b = r_0 B_0, \tag{A12}$$

and

$$x = \frac{r}{r_0}, \quad y = \frac{z}{r_0}. \tag{A13}$$

In terms of these new variables the partial differential equations (A1), (A3), (A4), (A6), (A7), and (A8) become, respectively,

$$\Delta^* u_1 = -u_2, \tag{A14}$$

$$\nu\Delta^* u_2 = \frac{I_b^2}{x^2}\frac{\partial u_3^2}{\partial y} - 2\frac{u_6 + I_e}{x^2}\frac{\partial u_5}{\partial y} + \frac{1}{x}\{u_6, u_5\} + \frac{1}{x}\{u_1, u_2\} + 2\frac{u_2}{x^2}\frac{\partial u_1}{\partial y} - I_b^2\frac{\partial}{\partial y}\left(\frac{u_4^2}{x^2}\right), \tag{A15}$$

$$\eta\Delta^* u_3 = \frac{2}{x^2}\left(u_3\frac{\partial u_1}{\partial y} - u_4\frac{\partial u_5}{\partial y}\right) + \frac{1}{x}(\{u_1, u_3\} + \{u_4, u_5\}), \tag{A16}$$

$$\nu\Delta^* u_4 = \frac{1}{x}(\{u_3, u_5\} + \{u_1, u_4\}), \tag{A17}$$

$$\Delta^* u_5 = -(u_6 + I_e), \tag{A18}$$

$$\eta u_6 = \frac{1}{x}\{u_5, u_1\}. \tag{A19}$$

The curly brackets denote the Poisson bracket of two functions u and v with respect to the variables x and y that is defined as

$$\{u, v\} = \frac{\partial u}{\partial x}\frac{\partial v}{\partial y} - \frac{\partial u}{\partial y}\frac{\partial v}{\partial x}. \tag{A20}$$

Equations (A14)–(A19) are subject to the following boundary conditions that follow from (15) and (16):
For $y = 0$

$$\begin{aligned} &\left.\frac{\partial u_3}{\partial y}\right|_{y=0} = 0, \quad \left.\frac{\partial u_5}{\partial y}\right|_{y=0} = 0, \quad \left.\frac{\partial u_6}{\partial y}\right|_{y=0} = 0, \\ &u_1|_{y=0} = 0, \quad u_2|_{y=0} = 0, \quad u_4|_{y=0} = 0. \end{aligned} \tag{A21}$$

For $x = x_- = r_-/r_0$, $x = x_+ = r_+/r_0$, and $y = y_+ = L/r_0$:

$$\begin{aligned} &u_1|_{x=x_\pm, y=y_+} = 0, \quad u_2|_{x=x_\pm, y=y_+} = 0, \\ &u_3|_{x=x_\pm, y=y_+} = 1, \quad u_5|_{x=x_\pm, y=y_+} = 0, \\ &u_6|_{x=x_\pm, y=y_+} = 0, \\ &\left.\frac{\partial u_4}{\partial x}\right|_{x=x_\pm} = \frac{2}{x_\pm}u_4|_{x=x_\pm}. \left.\frac{\partial u_4}{\partial y}\right|_{y=y_+} = 0. \end{aligned} \tag{A22}$$

The previously studied[8] "slow-flow" equations follow from Eqs. (A14) to (A19) by taking the high-viscosity limit ($H^2 \ll 1$). This results in

$$\Delta^* u_1 = -u_2, \tag{A23}$$

$$\nu\Delta^* u_2 = -2\frac{I_e}{x^2}\frac{\partial u_5}{\partial y}, \tag{A24}$$

$$\Delta^* u_5 = -I_e, \tag{A25}$$

with toroidal flow neglected. That is, u_4 is dropped, being a factor H^2 smaller than the poloidal flow variables u_1 and u_2, and the toroidal magnetic fields are ignored since $u_3 - 1$ is a factor H^2 smaller than the poloidal magnetic field variable u_5. The $\mathbf{v}\times\mathbf{B}$ force is also neglected, that is u_6 is dropped since it is of order H^2 compared to the current I_e that is driven by the externally applied electric field.

[1] J.A. Wesson, *Tokamaks* (Oxford University Press, Oxford, 1987).
[2] P.A. Sturrock, *Plasma Physics* (Cambridge University Press, Cambridge, 1994).
[3] R.J. Goldston and P.H. Rutherford, *Plasma Physics* (Institute of Physics, Bristol, 1995).
[4] J.A. Shercliff, *A Textbook on Magnetohydrodynamics* (Pergamon, Oxford, 1965).
[5] S.I. Braginskii, "Transport processes in a plasma," in *Reviews of Plasma Physics*, edited by M.A. Leontovich (Consultants Bureau, New York, 1965), Vol. 1.
[6] R. Balescu, *Transport Processes in Plasmas* (North–Holland, Amsterdam, 1988).
[7] D. Montgomery and X. Shan, Comments Plasma Phys. Controlled Fusion **15**, 315 (1994).
[8] D. Montgomery, J.W. Bates, and S. Li, Phys. Fluids **9**, 1188 (1997).
[9] L.P.J. Kamp, D.C. Montgomery, and J.W. Bates, Phys. Fluids **10**, 1757 (1998).

Downloaded 25 Sep 2008 to 131.155.151.77. Redistribution subject to AIP license or copyright; see http://pop.aip.org/pop/copyright.jsp

[10]J.W. Bates and D.C. Montgomery, Phys. Plasmas **5**, 2649 (1998), and references therein.
[11]D.C. Montgomery, J.W. Bates, and L.P.J. Kamp, Plasma Phys. Controlled Fusion **41**, A507 (1999).
[12]D.C. Montgomery, Plasma Phys. Controlled Fusion **34**, 1157 (1992).
[13]FEMLAB *Reference Manual*, *version 2.2* (COMSOL AB, Stockholm, Sweden, 2001).
[14]The JET Team, Nucl. Fusion **32**, 187 (1992).
[15]D.L. Book, *The NRL Plasma Formulary* (U.S. Naval Research Laboratory Publication 0084-4040, Washington, D.C., 1987).

Downloaded 25 Sep 2008 to 131.155.151.77. Redistribution subject to AIP license or copyright; see http://pop.aip.org/pop/copyright.jsp